Electrochimica Acta 340 (2020) 135980

Contents lists available at ScienceDirect

Electrochimica Acta

journal homepage: www.elsevier.com/locate/electacta

Hydrogen peroxide decomposition on simulated nuclear fuel bicarbonate/carbonate solutions

Ziyan Zhu [a], James J. Noël [a, b, *], David W. Shoesmith [a, b]

[a] Department of Chemistry, The University of Western Ontario, London, Ontario, N6A 5B7, Canada
[b] Surface Science Western, The University of Western Ontario, London, Ontario, N6C 0J3, Canada

ARTICLE INFO

Article history:
Received 24 January 2020
Received in revised form
23 February 2020
Accepted 25 February 2020
Available online 27 February 2020

Keywords:
Hydrogen peroxide
Uranium dioxide
Decomposition
UO_2 corrosion
SIMFUEL

ABSTRACT

The behavior of SIMFUEL (rare earth doped uranium dioxide containing noble metal particles) has been studied in bicarbonate/carbonate solutions (pH = 9.7) containing hydrogen peroxide, using a combination of electrochemical techniques, scanning electron microscopy (SEM), X-ray photoelectron spectroscopy (XPS), and inductively-coupled plasma mass spectrometry (ICP-MS). The hydrogen peroxide was found to decompose to oxygen and water both homogeneously and heterogeneously, accompanied by a minimal amount of corrosion of UO_2. Homogeneous decomposition proceeded via a peroxycarbonate (CO_4^{2-}) intermediate while heterogeneous decomposition was catalyzed by the reversible $U^{IV} \rightleftharpoons U^{V}$ redox transformation in a thin $U^{IV}_{1-2x}U^{V}_{2x}O_{2+x}$ surface layer. The rate of the heterogeneous decomposition reaction depended on whether U^{VI} surface species ($(U^{VI}O_2CO_3)_{ads}$, $U^{VI}O_3 \bullet yH_2O$) were allowed to accumulate on the surface, blocking access of hydrogen peroxide to the catalytic surface layer.

1. Introduction

In common with that of the international community, the Canadian strategy for the disposal of high-level nuclear waste is permanent disposal in a deep geologic repository (DGR), with the nuclear fuel waste sealed in a Cu-coated steel container [1–3]. These containers are expected to avoid failure until the fuel radiation levels have decayed to innocuous levels [4]. However, to develop robust performance assessment models for a DGR, it is necessary to examine the consequences of container failure, when the used fuel could come into contact with groundwater, potentially leading to the release of radionuclides from the fuel matrix. Although the groundwater entering the container would be anoxic, the redox conditions within the container, which will control the rate of release of most radionuclides from the fuel, will be controlled by the products of groundwater radiolysis and corrosion of the inner surface of the steel container [5,6]. Of the radiolytic oxidants, H_2O_2 is expected to have the dominant influence on fuel corrosion [7,8].

The influence of H_2O_2 on UO_2 corrosion has been extensively studied and reviewed [5,9,10]. On the UO_2 surface two competing anodic reactions which can couple with the cathodic reduction of H_2O_2 are the oxidative dissolution of $U^{IV}O_2$ as $U^{VI}O_2^{2+}$ and the oxidation of H_2O_2, the latter leading to the net decomposition of H_2O_2:

$$2H_2O_2 \rightarrow O_2 + 2H_2O \quad (1)$$

Peroxide decomposition has been studied on various metal oxides [5], and a number of reaction sequences proposed. Recent studies claim that decomposition proceeds via a radical mechanism [11–13]:

$$(H_2O_2)_{ads} \rightarrow 2(OH^{\bullet})_{ads} \quad (2)$$

$$(H_2O_2)_{ads} + (OH^{\bullet})_{ads} \rightarrow H_2O + (HO_2^{\bullet})_{ads} \quad (3)$$

$$2(HO_2^{\bullet})_{ads} \rightarrow H_2O_2 + O_2 \quad (4)$$

Decomposition on oxides can be catalyzed by reversible redox transformations [14,15]. On $U^{IV}O_2$ surfaces, the balance between $U^{IV}O_2$ dissolution and H_2O_2 decomposition varied depending on the surface composition of the oxide. Thus, 14% of the H_2O_2 was consumed by dissolution on $U^{IV}O_2$ surfaces, compared to ~2% on SIMFUEL [16] ($U^{IV}O_2$ doped with non-radioactive elements, including rare earth elements, to simulate in-reactor burn-up [17]).

* Corresponding author. Department of Chemistry, The University of Western Ontario, London, Ontario, N6A 5B7, Canada.
E-mail address: jjnoel@uwo.ca (J.J. Noël).

https://doi.org/10.1016/j.electacta.2020.135980

This difference has been attributed to differences in the redox reactivities of these two oxides [8], although the presence of potentially catalytic noble metal (ε) particles in the SIMFUEL was not addressed. The stabilization of the $U^{IV}O_2$ matrix against dissolution, by the rare earth doping present in SIMFUEL, has been demonstrated electrochemically [18–21]. Corrosion potential (E_{CORR}) measurements indicate that the decomposition of H_2O_2 may be controlled by the kinetics of the H_2O_2 reduction [22].

In this study we have investigated the reactions of, and on, SIMFUEL in NaCl solutions containing various concentrations of HCO_3^-/CO_3^{2-} and H_2O_2. The primary emphasis is on determining the mechanisms and relative importance of $U^{IV}O_2$ dissolution and H_2O_2 decomposition. A combination of electrochemical, and surface and solution analytical methods such as X-ray photoelectron spectroscopy (XPS), scanning electron microscopy (SEM), energy dispersive X-ray analysis (EDX), inductively coupled plasma mass spectrometry (ICP-MS) and UV–vis spectrophotometry, have been applied.

2. Experimental

2.1. Materials

The UO_2 electrodes were cut from 3 at.% SIMFUEL manufactured by Atomic Energy Canada Limited (now Canadian Nuclear Laboratories, Chalk River, Ontario, Canada). SIMFUELs are $U^{IV}O_2$ pellets doped with 11 non-radioactive elements (Ba, Ce, La, Sr, Mo, Y, Zr, Rh, Pd, Ru, Nd) to replicate the chemical effects of in-reactor irradiation, and have been well characterized and studied [17]. These dopants are categorized into two groups: (1) elements which are distributed throughout the $U^{IV}O_2$ matrix and can influence the structure and electrical conductivity; and (2) elements (Pd, Ru, Rh, Mo) which segregate as noble metal (ε) particles and are generally distributed along grain boundaries. The distribution and composition of these particles has been described elsewhere [23,24].

2.2. Electrodes and solutions

Electrodes were polished on wet 1200 SiC paper and rinsed with Type I water prior to experiments. All solutions were prepared with Type I water (ρ = 18.2 MΩ cm), purified using a Millipore Milli-Q Plus unit and deaereated by Ar (ultra-high purity, Praxair) sparging (>1 h) prior to each experiment. Sparging was then continued throughout each experiment. Experiments were performed in a 0.1 mol L^{-1} NaCl solution containing $NaHCO_3$ (0.005–0.05 mol L^{-1}) and H_2O_2 (0.001 mol L^{-1} to 0.02 mol L^{-1}), with the pH adjusted to 9.7 using 0.2 mol L^{-1} NaOH solution, and measured using an Orion model 250A pH meter and an Orion 91-07 Triode pH/ATC probe. All chemicals were reagent grade and purchased from Fisher Scientific. All experiments were performed at room temperature.

2.3. Electrochemical cell and procedures

A one-compartment 40 mL cell was used to minimize the UO_2 surface area to solution volume ratio, enabling more accurate measurements of H_2O_2 consumption and U dissolution. Potentials were measured against a saturated Ag/AgCl reference electrode placed in the main cell compartment. A Pt wire counter electrode was used, separated from the main cell body by a high-density glass frit. Experiments were performed in a Faraday cage to minimize interference from external electrical noise, and the cell was covered with Al foil to avoid photolytic decomposition of the H_2O_2. All electrochemical experiments were performed using a Solartron 1480 Multistat controlled by CorrWare Version 2.7 software.

Prior to each experiment, the electrode was polarized to −1.2 V (vs. saturated Ag/AgCl) for 20 s to cathodically reduce air-formed oxides. Polarization resistances (R_P) were obtained from the slopes of current-potential scans over the range E_{CORR} ± 10 mV. Electrodes for XPS analyses were removed from the cell, rinsed with Type 1 water, dried in an Ar stream, and immediately sealed in an evacuated plastic box for rapid transfer to the spectrometer.

2.4. SEM and EDX

The surface morphology of electrodes was observed using a Hitachi S-4500 field emission SEM equipped with a Quartz XOne EDX analysis system. An electron beam voltage of 20 kV was used at a working distance of 10 mm during image collection, resulting in a spatial resolution of <2 nm.

2.5. XPS

XPS analyses were performed using a Kratos Axis NOVA spectrometer with a monochromatic Al K_α X-ray source (1486.6 eV). The instrument work function was calibrated to give a BE of 83.96 eV for the Au $4f_{7/2}$ line for metallic Au and the spectrometer dispersion was adjusted to give a BE of 932.62 eV for the Cu $2p_{3/2}$ line of metallic Cu. Survey scans were recorded over the energy range 0–1100 eV on an analysis area of 300 × 700 μm^2 with a pass energy of 160 eV. When necessary, spectra were charge-corrected using the C 1s peak set at 285.0 eV. Spectra were analyzed using CasaXPS software (version 2.3.14).

High resolution scans were performed for the spectral region including the U $4f_{5/2}$ and U $4f_{7/2}$ peaks and their satellites, using a pass energy of 20 eV and a step size of 0.05 eV. All spectra were fitted using a 50% Gaussian and 50% Lorentzian routine with a Shirley background correction. The 4f peaks were used to quantify the U oxidation states (U^{IV}, U^{V}, U^{VI}) using curve-fitting procedures and binding energies discussed elsewhere [25–27]. The resolved components in both the U 4f peaks and the associated satellite structures were used to calculate the total proportions of each oxidation state. The positions and shapes of the satellite structures were used to confirm the validity of the analyses, as described in published literature [28–31].

2.6. ICP-MS

Dissolved U concentrations were determined by ICP-MS with an Agilent 7700 x ICP-MS using both “He gas” and “No gas” modes. Solutions were diluted by a factor of 1000 using 2% HNO_3 prior to analysis to minimize matrix effects. The detection limit was 0.02 μg/L for U and the system was calibrated using a series of U standards.

2.7. UV–vis spectrophotometry

H_2O_2 concentrations were measured with a BioLogic Science Instrument MOS 450 diode array UV–vis Spectrophotometer using the Ghormley tri-iodide method [32,33]. The absorbance at 352 nm was measured with a detection limit for H_2O_2 of 3 x 10^{-6} mol L^{-1}. Analyses were performed immediately after sampling, with the vial containing the extracted solution covered with Al foil.

3. Results

3.1. SEM/EDX analysis

Fig. 1 shows the surface morphology of a freshly polished and sonicated 3 at.% SIMFUEL with noble metal (ε) particles. In Fig. 1(A), area (a) shows the general surface to be rough with residual

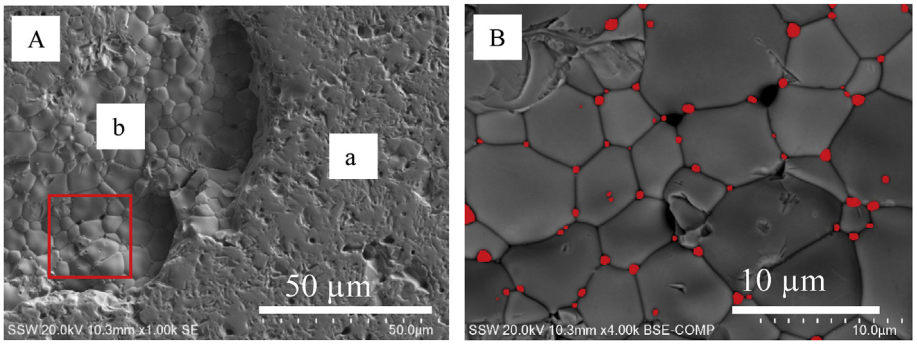

Fig. 1. SEM images of a 3 at.% SIMFUEL specimen. A: (a) the polished surface; (b) smooth, large UO_2 grains, untouched by the polishing procedure: B: showing the presence of ε-particles on the grain boundaries (highlighted in red to emphasize their locations): image B is the magnification of the area within the red box in image (A).

sintering voids. Locations untouched by polishing, area (b), show undamaged UO_2 grain features. Fig. 1(B) shows that the UO_2 consists of large and smooth grains with diameters in the range 3–10 µm. The small particles decorating the grain boundaries, highlighted in red, have been shown previously to be noble metal (ε) particles containing Mo, Pd, Ru and Rh [23,24].

3.2. Hydrogen peroxide decomposition in HCO_3^-/CO_3^{2-} solutions

The effect of HCO_3^-/CO_3^{2-} on the homogeneous decomposition of H_2O_2 is shown in Fig. 2. In the absence of HCO_3^-/CO_3^{2-}, the $[H_2O_2]$ decreased by ~ 10% in 7 days, consistent with published data showing that H_2O_2 decomposition occurs in alkaline solutions with or without the presence of metal catalysts [34–38]. Littauer et al. [38] proposed that decomposition in alkaline (pH = 12) solutions occurs via the formation of perhydroxyl ions (HO_2^-), which then catalyze H_2O_2 decomposition via reactions 5 and 6:

$$H_2O_2 + OH^- \rightarrow HO_2^- + H_2O \quad (5)$$

$$HO_2^- + OH^- \rightleftharpoons O_2 + H_2O + 2e^- \quad (6)$$

In the absence of metallic or oxide catalysts[36], the rate of decomposition is determined by both the total alkalinity and

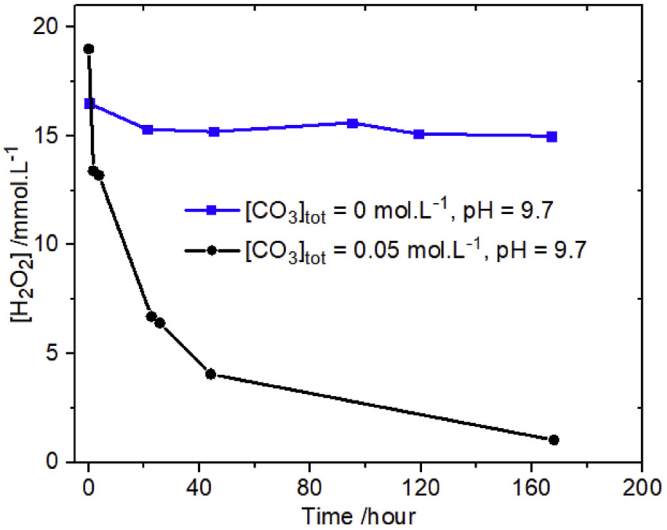

Fig. 2. H_2O_2 concentration as a function of time: $[H_2O_2] = 0.016$ mol L^{-1} in both experiments (pH adjusted to 9.7).

$[H_2O_2]$.

In the HCO_3^-/CO_3^{2-} solution, the $[H_2O_2]$ decreased markedly over the 168-h duration of the experiment, demonstrating a catalytic influence of HCO_3^-/CO_3^{2-} aside from any influence of alkalinity. Raman spectroscopy has been used to demonstrate the formation of peroxycarbonate ions when HCO_3^-/CO_3^{2-} is present in H_2O_2 solutions in the pH range 7.0–9.5 [39]. The H_2O_2 decomposition rate in HCO_3^-/CO_3^{2-} solutions achieves a maximum at pH values between 11.5 and 11.7 [40], when the solution carbonate is dominantly in the form of CO_3^{2-}. It was proposed that the reaction proceeded via steps 7 and 8:

$$CO_3^{2-} + H_2O_2 \rightarrow CO_4^{2-} + H_2O \quad (7)$$

$$CO_4^{2-} + HO_2^- \rightarrow HCO_3^- + H_2O + O_2 \quad (8)$$

At the pH of 9.7 used in our experiments, the solution carbonate would have been ~40% in the form of CO_3^{2-}, making it essential to consider the homogeneous decomposition process when evaluating the influence of $U^{IV}O_2$ on the heterogeneous decomposition of H_2O_2.

3.3. H_2O_2 decomposition on SIMFUEL

In the presence of SIMFUEL, the total decrease in $[H_2O_2]$ ($\Delta[H_2O_2]_{tot}$) can be attributed to a combination of both homogeneous decomposition in solution ($\Delta[H_2O_2]_{sol}$) and reactions on the SIMFUEL surface ($\Delta[H_2O_2]_{UO2}$). These latter reactions include both heterogeneous decomposition and consumption by $U^{IV}O_2$ corrosion. The total amount decomposed ($\Delta[H_2O_2]_{tot}$) can be corrected for homogeneous decomposition by comparing H_2O_2 consumption in the presence and absence of a SIMFUEL electrode, and is given by:

$$\Delta[H_2O_2]_{UO2} = \Delta[H_2O_2]_{tot} - \Delta[H_2O_2]_{sol} \quad (9)$$

In a solution containing $[H_2O_2] = 0.01$ mol L^{-1} and $[CO_3]_{tot} = 0.05$ mol L^{-1}, Fig. 3(A), approximately 48% of the available H_2O_2 was consumed, with 14% consumed by homogeneous decomposition ($\Delta[H_2O_2]_{sol}$), and the majority by either decomposition on, or reaction with, the SIMFUEL ($\Delta[H_2O_2]_{UO2}$). Reducing the $[CO_3]_{tot}$ by a factor of 5 to 0.01 mol L^{-1} almost eliminated homogeneous decomposition, Fig. 3(B), confirming the dependence of this reaction on $[CO_3^{2-}]$. In this solution, while reaction on the SIMFUEL surface was the dominant process, the overall consumption of H_2O_2 was decreased. A comparison of the results in Fig. 3A and B indicates a significant role for HCO_3^-/CO_3^{2-} in accelerating the

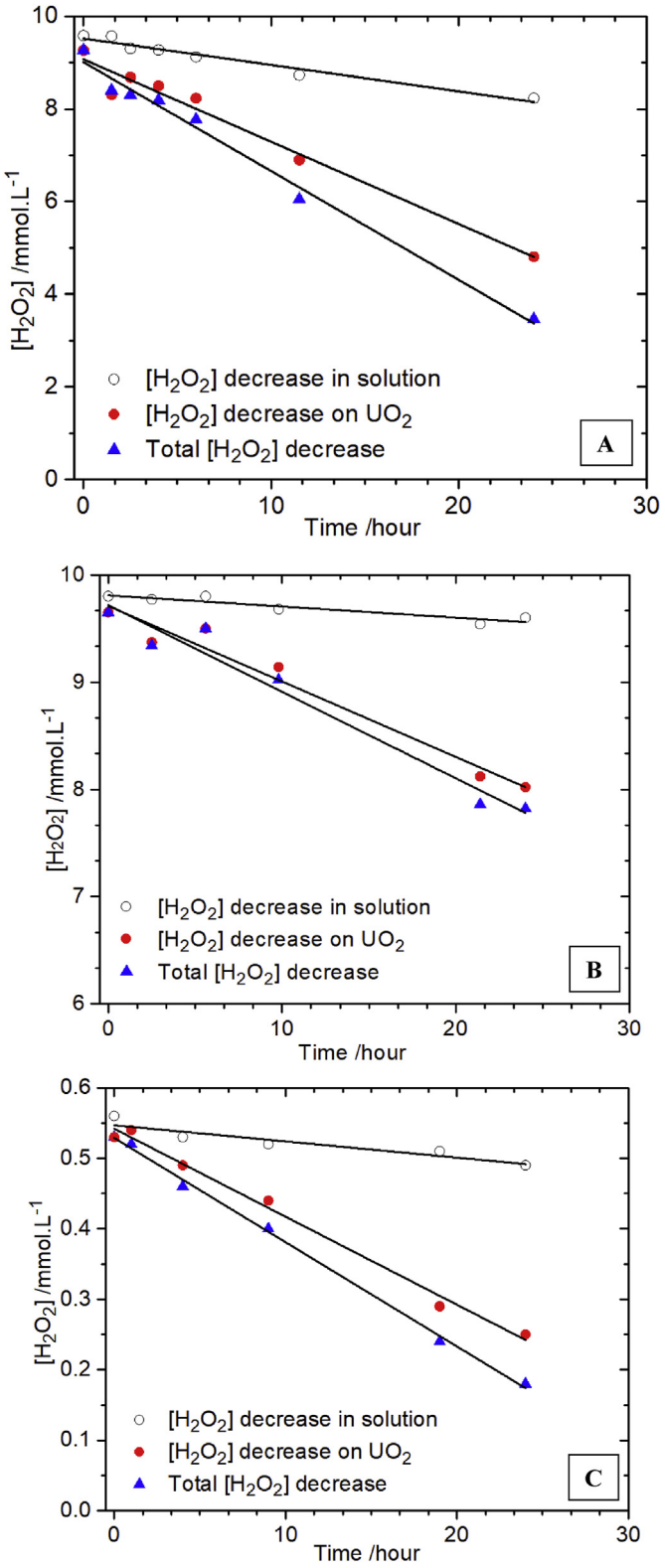

Fig. 3. $[H_2O_2]$ as a function of time in solutions containing various $[H_2O_2]$ and $[CO_3]_{tot}$; Hollow circle – no SIMFUEL present; blue triangle – SIMFUEL present; Red circle – decrease in $[H_2O_2]$ by reaction on SIMFUEL. (A) $[H_2O_2]$ = 0.01 mol L^{-1}, $[CO_3]_{tot}$ = 0.05 mol L^{-1}; (B)) $[H_2O_2]$ = 0.01 mol L^{-1}, $[CO_3]_{tot}$ = 0.01 mol L^{-1}; (C)) $[H_2O_2]$ = 0.0005 mol L^{-1}, $[CO_3]_{tot}$ = 0.05 mol L^{-1}. All the solutions contained 0.1 mol L^{-1} of NaCl, pH = 9.7. (For interpretation of the references to colour in this figure legend, the reader is referred to the Web version of this article.)

reactions on the SIMFUEL surface. At a higher $[CO_3]_{tot}$, but lower $[H_2O_2]$, the fractions of the H_2O_2 consumed homogeneously and heterogeneously, Fig. 3(C), were similar to those observed at the same $[CO_3]_{tot}$ and higher $[H_2O_2]$, Fig. 3(A). These results confirm the importance of HCO_3^-/CO_3^{2-} in both the homogeneous and heterogeneous reactions.

3.4. E_{CORR} and R_P Measurements

In a series of experiments conducted in 0.1 mol L^{-1} NaCl containing various $[CO_3]_{tot}$ and $[H_2O_2]$, the E_{CORR} was monitored over an exposure period of 24 h, and a series of R_P measurements performed at 1-h intervals. Three examples of the change in E_{CORR} and R_P with time are shown in Fig. 4. In all three experiments, E_{CORR} rapidly increased to ~0.15 V (not observable on the plots) before decaying to less positive values, while R_P values decreased over approximately the first 5 h before increasing steadily over the remaining exposure period.

The anodic oxidation of both UO_2 and H_2O_2 is supported by the cathodic reduction of H_2O_2,

$$I_{CORR} + I_{H2O2} = \sum I_A = I_{Cw} \quad (10)$$

here I_{CORR} is the current due to $U^{IV}O_2$ dissolution and I_{H2O2} that due to the anodic oxidation of H_2O_2. However, since R_P^{-1} is proportional to the total interfacial charge transfer rate, it does not distinguish between the relative rates of the two reactions.

The initial decrease in R_P indicated an acceleration of the interfacial reaction rate over the first ~5 h. A decrease in E_{CORR}, Fig. 4(A, B, C), coupled with a decrease in R_P indicates an acceleration of one or both the anodic reactions. Fig. 5 shows a plot of $\Delta E_{CORR}/\Delta R_P$ as a function of $[H_2O_2]$ in a solution containing 0.05 mol L^{-1} $[CO_3]_{tot}$, where Δ indicates the change in these two parameters over the initial exposure period of 1–5 h. Since R_P values were measured over a small potential range, within which the current varies linearly with applied potential, $\Delta E_{CORR}/\Delta R_P$ is proportional to the total interfacial current, $I_{CORR} + I_{H2O2}$. The increase in this parameter with $[H_2O_2]$ demonstrates that the rate of the overall anodic reaction increases as $[H_2O_2]$ increases. Although limited to $[H_2O_2] < 0.02$ mol L^{-1}, this rate parameter continues to increase with $[H_2O_2]$, but the small changes in R_P make the values of ΔR_P unreliable.

At longer exposure times, the decrease in E_{CORR}, coupled with an increase in R_P, Fig. 4, indicates a change in the reaction controlling the interfacial kinetics to the cathodic reduction of H_2O_2. This can be attributed to the consumption of H_2O_2, as demonstrated in Fig. 3.

Comparison of Fig. 4(A) and (B) shows the influence of changing the $[CO_3]_{tot}$ by a factor of 5 in solutions containing the same $[H_2O_2]$ (0.01 mol L^{-1}). In the more concentrated HCO_3^-/CO_3^{2-}, Fig. 4(A), E_{CORR} decreases steadily as H_2O_2 is consumed, Fig. 3(A). At the lower $[CO_3]_{tot}$, Fig. 4(B), the decrease in E_{CORR} and long-term increase in R_P are relatively small, consistent with a lower rate of H_2O_2 consumption, Fig. 3(B). Despite the identical $[H_2O_2]$, the overall rate of its consumption (R_P^{-1}) was lower at lower $[CO_3]_{tot}$.

Since we would not expect HCO_3^-/CO_3^{2-} to have any major influence on the rate of H_2O_2 decomposition on noble metal particles, the difference in H_2O_2 consumption rate can be attributed to the influence of HCO_3^-/CO_3^{2-} on the rate of the processes occurring on the $U^{IV}O_2$ surface. Lower E_{CORR} values, coupled with increased interfacial rates ($\propto R_P^{-1}$), indicated that the dominant effect of an increase in $[CO_3]_{tot}$ was to accelerate the rate of one or both of the anodic reactions. This hypothesis appears to be borne out by the values recorded at high $[CO_3]_{tot}$/low $[H_2O_2]$, Fig. 4(C), the E_{CORR}/R_P behavior being similar to that recorded at high $[CO_3]_{tot}$/high $[H_2O_2]$, with the exception that that R_P values are considerably higher at the

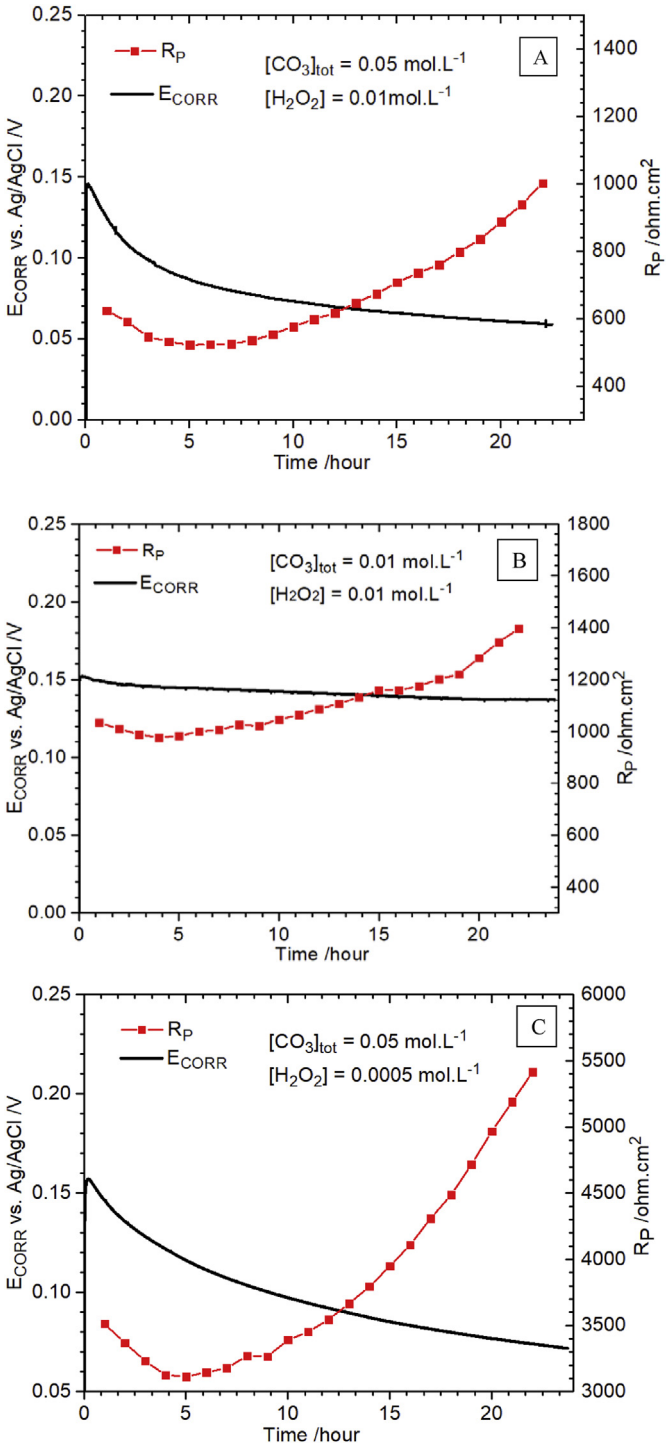

Fig. 4. Corrosion potential (E_{CORR}) and polarization resistance (R_P) measurements as a function of time in solutions containing different $[H_2O_2]$ and $[CO_3]_{tot}$. The curves show E_{CORR} (black line) and the connected squares show the R_P values measured every hour. All the solutions contain 0.1 mol L^{-1} of NaCl (pH = 9.7).

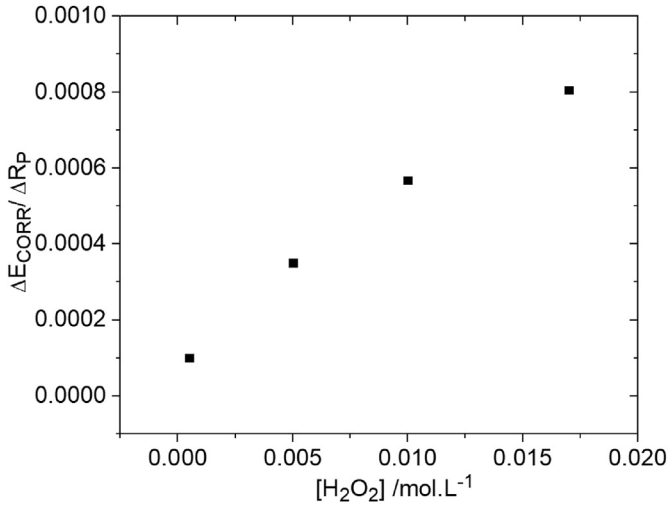

Fig. 5. The ratio of the E_{CORR} over R_P value change within 5 h in solutions containing 0.1 mol L^{-1} NaCl, 0.05 mol L^{-1} $NaHCO_3$, various concentrations of H_2O_2, and pH = 9.7.

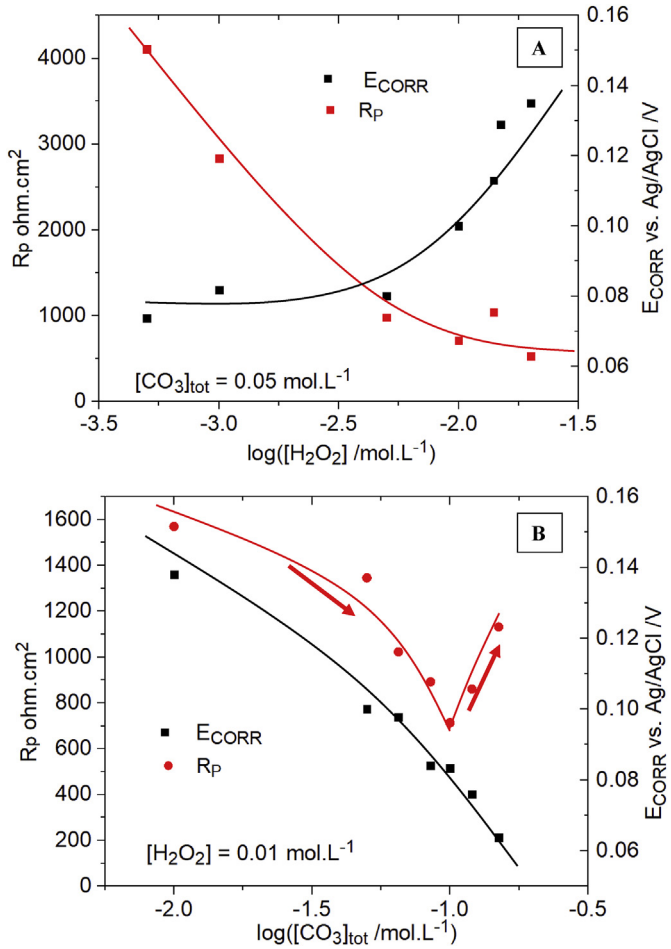

Fig. 6. R_P and E_{CORR} values recorded after 16 h of exposure: A-as a function of $[H_2O_2]$; B-as a function of $[CO_3]_{tot}$. All the solutions contained 0.1 mol L^{-1} of NaCl, pH = 9.7.

lower $[H_2O_2]$.

Fig. 6(A and B) show the changes in R_P and E_{CORR} recorded over a wider range of $[H_2O_2]$ (A) and $[CO_3]_{tot}$ (B), with the values recorded after 16 h, when the initial acceleration in the rate is complete and before the H_2O_2 becomes too extensively depleted. The interfacial reaction rate (R_P^{-1}), the rate of H_2O_2 consumption, increases rapidly with increasing $[H_2O_2]$ at low $[H_2O_2]$, while E_{CORR} remains effectively constant. At higher $[H_2O_2]$, the rate approaches a concentration-independent value, while E_{CORR} increases markedly. Since these experiments were conducted in a solution containing 0.05 mol L^{-1} HCO_3^-/CO_3^{2-}, the electrode surface should be relatively

free of U^{VI} species (see below), allowing H_2O_2 consumption to proceed uninhibited.

Similar changes in E_{CORR} with $[H_2O_2]$ were observed previously on an undoped UO_2 not containing noble metal (ε) particles [9], suggesting that the present observations could be attributed to reactions occurring predominantly on the UO_2 surface, not on the noble metal (ε) particles. Although no rates were measured in this previous study, it was proposed that the behavior at low $[H_2O_2]$, when E_{CORR} was independent of $[H_2O_2]$, could be attributed to the dominance of H_2O_2 decomposition over UO_2 corrosion, with the increase in E_{CORR} at higher $[H_2O_2]$ indicating an increased importance of the anodic dissolution of UO_2. The results presented here show that if such a change in the importance of the individual reactions occurred at higher $[H_2O_2]$, it did not lead to any increase in the consumption rate of H_2O_2.

The influence of $[CO_3]_{tot}$ on E_{CORR} and the interfacial rate involves two distinct stages, Fig. 6(B). While E_{CORR} decreases over the full concentration range investigated, the consumption rate first increases with $[CO_3]_{tot}$ (for concentrations $\leq$ 0.1 mol L^{-1}) before decreasing again at higher $[CO_3]_{tot}$ (as indicated by the arrows in the figure).

3.5. XPS analysis of UO_2 surface composition

Previous studies have shown that the extent of oxidation of a UO_2 surface during corrosion is confined to the top few nanometres [5,9,18–20]. Consequently, XPS spectra were recorded on SIMFUEL specimens exposed to solutions containing 0.01 mol L^{-1} H_2O_2 and two different $[CO_3]_{tot}$. Fig. 7 shows the background-corrected and fitted U $4f_{7/2}$ peaks, deconvoluted to determine the relative amounts of U^{IV}, U^V and U^{VI} in the electrode surface. The exposure times were chosen to yield measurements of surface composition after the initial acceleration in the interfacial rate (4 h, Fig. 4) and after an extended exposure period (16 h, Fig. 4), when the interfacial rate had slowed due to the consumption of H_2O_2. Fig. 8 compares the fractions of the individual oxidation states (expressed as percentages) in the exposed electrode surfaces to values measured on a freshly polished, electrochemically reduced surface.

For the freshly polished and reduced electrode, only minor amounts of oxidized states (U^V and U^{VI}) were present, as expected after this treatment. After exposure to the more concentrated HCO_3^-/CO_3^{2-} solution (0.05 mol L^{-1}), the U^V content of the surface increased substantially after 4 h, and even more so after 16 h, while the U^{VI} content remained minor, i.e., this increase in U^V content is at the expense of U^{IV}. When considered in conjunction with the R_P values for a high $[CO_3]_{tot}$/high $[H_2O_2]$ solution (Fig. 4(A)), these analyses showed that an increase in rate (decrease in R_P) accompanied this initial oxidation of the surface to $U^{IV}_{1-2x}U^V_{2x}O_{2+x}$, and that a predominantly U^{IV}/U^V surface is sustained at longer times when consumption of H_2O_2 proceeded, as indicated by the increase in R_P. These results confirm that the optimum surface composition to support H_2O_2 decomposition is a mixed U^{IV}/U^V surface. This offers strong evidence that the decomposition reaction is catalyzed by a reversible U^{IV}-U^V redox transformation in the $U^{IV}O_2$ surface, with the dependence of R_P on E_{CORR} in the exposure period from 1 h to 5 h indicating that this leads to an acceleration of the overall anodic reaction, but without indicating which of the two possible anodic reactions might be influenced most.

When the $[CO_3]_{tot}$ was reduced by an order of magnitude, the surface after 4 h again exhibited a significant U^V content, consistent with the formation of the $U^{IV}_{1-2x}U^V_{2x}O_{2+x}$ layer, but also contained

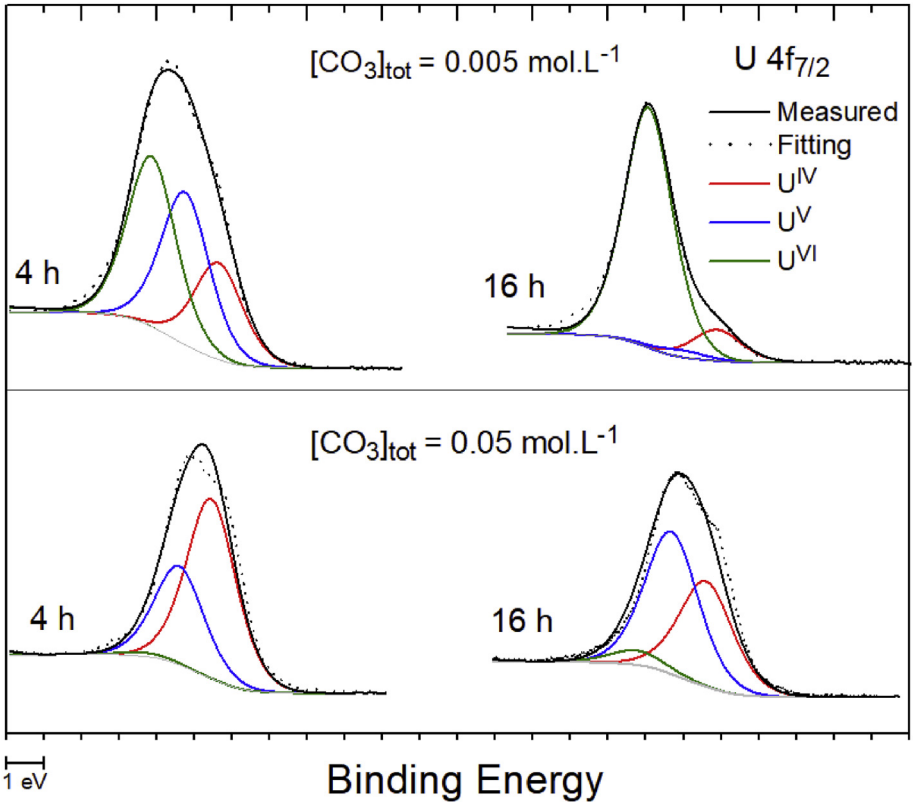

Fig. 7. The U $4f_{7/2}$ peak recorded on SIMFUEL surfaces (dashed line), deconvoluted into contributions from U^{IV}, U^V and U^{VI}, after various periods of exposure to solutions containing different 0.01 mol L^{-1} H_2O_2 and HCO_3^-/CO_3^{2-} concentrations. All solutions contained 0.1 mol L^{-1} NaCl (pH = 9.7).

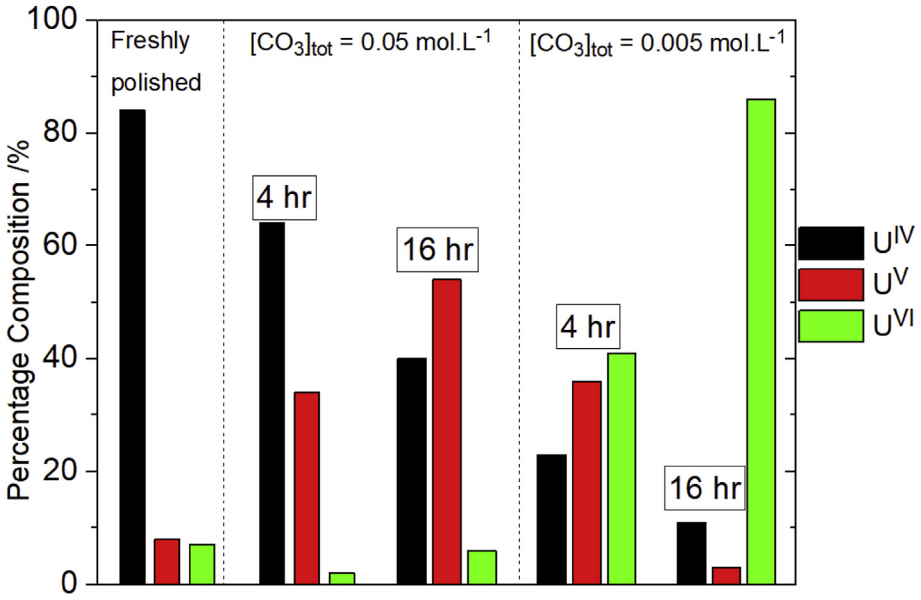

Fig. 8. Percentage of U oxidation states in the SIMFUEL surface after exposure to a 0.01 mol L^{-1} H_2O_2 solution, obtained by deconvolution of the U $4f_{7/2}$ peaks in the XPS spectra, Fig. 7.

a substantial U^{VI} content. After 16 h, the surface composition was totally dominated by U^{VI}. When considered in conjunction with the R_P values recorded in the low $[CO_3]_{tot}$/high $[H_2O_2]$ solution (Fig. 4(B)), these analyses showed that, while the initial formation of the U^{IV}/U^{V} layer accelerated the consumption of H_2O_2, it was muted and eventually suppressed by the accumulation of U^{VI} surface species at longer exposure times. This would account for the small increase in R_P accompanied by only a marginal decrease in E_{CORR} (Fig. 4(B)).

3.6. UO_2 dissolution experiments

Up to this juncture, only the overall consumption of H_2O_2 was measured. To determine the relative importance of the two reactions responsible for H_2O_2 consumption, a series of experiments was conducted, over an exposure period of 24 h, to determine the amount of dissolved U and the total amount of H_2O_2 consumed. The analyzed amount of U was then used to calculate the fraction of the consumed H_2O_2 used in UO_2 corrosion. The O_2 produced by decomposition could also have acted as an oxidant for UO_2, but at a rate 200 times slower than H_2O_2 [41]. This low rate, and the continuous sparging of the solution with Ar, meant that any influence of O_2 could be neglected. The surface films formed ($U^{IV}_{1-2x}U^{V}_{2x}O_{2+x}$, U^{VI} oxide/hydroxide/carbonate) would also have consumed negligible amounts of H_2O_2 in their formation since they were, at most, only a few nanometres thick.

Fig. 9 shows the influence of $[CO_3]_{tot}$ on U dissolution over a 24 h exposure period in a solution containing 0.01 mol L^{-1} H_2O_2. At high $[CO_3]_{tot}$ (35–100 mmol L^{-1}), the amount of U released increased over the first ~ 10 h, before the release stopped. At lower $[CO_3]_{tot}$, U release, while somewhat erratic, tended to continue unabated. At the higher $[CO_3]_{tot}$, the duration of the short-term release coincided with the exposure period over which R_P values decreased, indicating an acceleration in H_2O_2 consumption as the surface was oxidized to the $U^{IV}_{1-2x}U^{V}_{2x}O_{2+x}$ catalytic composition. At the lower $[CO_3]_{tot}$, when the U release was sustained, the rate of H_2O_2 consumption was substantially lower, Figs. 3(B) and 4(B), and the XPS analyses show that the surface became partially blocked by the accumulation of U^{VI}.

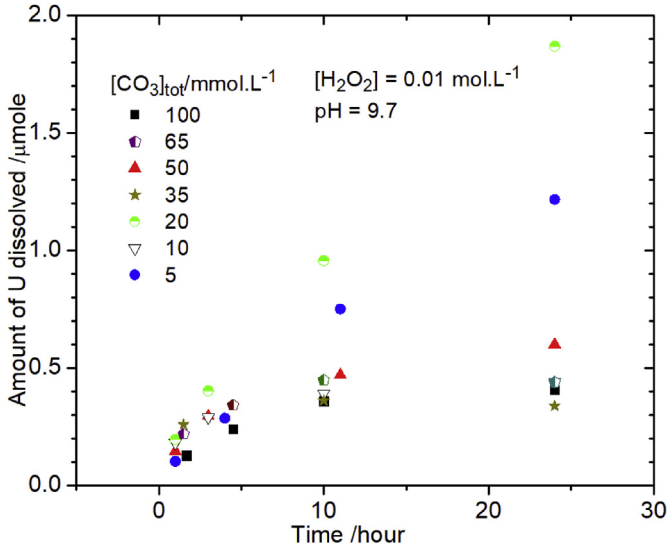

Fig. 9. The amount of dissolved U measured as a function of time in 0.01 mol L^{-1} H_2O_2 solutions containing different $[CO_3]_{tot,}$ as a function of time.

Table 1 shows the ratio of the amount of H_2O_2 causing dissolution to the total amount consumed, corrected for that consumed by homogeneous decomposition. These fractions confirm that the great majority of H_2O_2 was consumed by decomposition, with only

Table 1
The amount U dissolved in different $[CO_3]_{tot}$ solutions and the calculated fraction of H_2O_2 used to oxidize U ($[H_2O_2]_{dis}$) over the total $[H_2O_2]$ ($[H_2O_2]_{tot}$).

$[CO_3]_{tot}$ (mmol.L^{-1})	U dissolved in 24 h (µmol)	$[H_2O_2]_{dis}/[H_2O_2]_{UO2}$ (%)
5	1.2	3.1
20	1.8	4.1
35	0.34	0.23
50	0.6	0.76
65	0.44	2.0
100	0.4	0.3

a small fraction used to cause UO_2 corrosion. These results were consistent with those of Nilsson et al. [16], who found that only 0.2% of the H_2O_2 consumed on a SIMFUEL surface caused UO_2 dissolution.

4. Discussion

In aqueous HCO_3^-/CO_3^{2-} solutions containing a SIMFUEL specimen (electrode), decomposition was the dominant route for H_2O_2 consumption. This process proceeded both homogeneously and heterogeneously. Under the conditions employed in the present study (pH = 9.7, 0.005 mol $L^{-1} \leq [CO_3]tot \leq$ 0.2 mol L^{-1}; 0.001 mol $L^{-1} \leq [H_2O_2] \leq$ 0.02 mol L^{-1}), approximately 10−15% of the H_2O_2, depending on $[CO_3]_{tot}$, was decomposed homogeneously via the formation of a peroxycarbonate (CO_4^{2-}) intermediate (reactions 7 and 8). These reactions are strongly dependent on pH and would be less significant at a lower pH value.

The dominant reaction consuming H_2O_2 was its catalytic decomposition on the SIMFUEL surface, only a small fraction (<4%, depending on $[CO_3]_{tot}$) being consumed by UO_2 corrosion for a $[H_2O_2]$ of 0.01 mol L^{-1}. These values were consistent with those measured by Nilsson et al. [16] and considerably lower than the 14% measured on undoped UO_2 containing no noble metal particles. This difference has been shown to be due to the rare earth (RE^{III}) doping of the UO_2 lattice, which leads to the formation of RE^{III}-O_V clusters and a reduction in the availability of the oxygen vacancies (O_V) required to accommodate the incorporation of the O interstitial ions which begin the process of destabilizing the UO_2 matrix [19,20,42].

On first immersion, the reduced SIMFUEL surface was oxidized to $U^{IV}_{1-2x}U^{V}_{2x}O_{2+x}$, at a rate determined by the $[H_2O_2]$. This reaction preceded the eventual further oxidation and dissolution as $U^{VI}O_2^{2+}$ [29,43]. However, such a dissolution process was transitory, with decomposition becoming the sole observable reaction after a few hours. The formation of this layer was accompanied by a decrease in E_{CORR} and an increase in the H_2O_2 decomposition rate. This combination, and the switching off of the U release to solution, indicated a depolarization of the anodic dissolution reaction to produce $U^{VI}O_2^{2+}$ and demonstrated that the overall decomposition reaction, which proceeds via radical intermediates (reactions 2 to 4), was catalyzed by the reversible redox transformation occurring on the $U^{IV}_{1-2x}U^{V}_{2x}O_{2+x}$ surface; i.e., reactions 1 and 2 in the schematic illustration in Fig. 10. This would require that the reduction of U^{V} to U^{IV} (reaction 2, Fig. 10) was more rapid than its further oxidation to U^{VI} via the sequence of reactions leading to dissolution as $U^{VI}O_2(CO_3)_y^{(2-2y)+}$ (reactions 3 to 5, Fig. 10).

The E_{CORR} and R_P measurements demonstrated that the rate of decomposition was accelerated by an increase in $[CO_3]_{tot,}$ except at high $[CO_3]_{tot}$ (>0.1 mol L^{-1}). The primary function of HCO_3^-/CO_3^{2-} was to complex and dissolve surface U^{VI} species ($(U^{VI}O_2CO_3)_{ads}$) formed by oxidation of the catalytic surface (reactions 4 and 5,Fig. 10), preventing their accumulation on, and blockage of, the catalytic surface sites. It was also possible (but not shown in Fig. 10) that heterogeneous decomposition involved the peroxycarbonate species (CO_4^{2-}) formed in the solution, which has been shown to be readily oxidizable on SIMFUEL surfaces.

At high $[CO_3]_{tot}$ (>0.1 mol L^{-1}) (Fig. 6(B)), the decrease in decomposition rate with increasing $[CO_3]_{tot}$ was most likely due to the more rapid formation of the surface-adsorbed carbonate complex state on the $U^{IV}_{1-2x}U^{V}_{2x}O_{2+x}$ surface (reactions 3 and 4, Fig. 10) [44]. This would facilitate the release of U^{VI}, a reaction controlled by the chemical dissolution of U^{VI} surface species (reaction 5, Fig. 10). This sequence of reactions would have extracted the U^{V} species from the catalytic surface layer by anodic oxidation and inhibited the matrix reduction reaction (reaction 2, Fig. 10) required to complete the decomposition process.

When the $[CO_3]_{tot}$ became too low to prevent the accumulation of U^{VI} species on the catalytic surface layer, Fig. 7, H_2O_2 consumption was suppressed, as shown by the R_P values in Fig. 6(B). Under these conditions, the surface U^{VI} species was likely to be a uranyl oxide, $U^{VI}O_3 \cdot 2H_2O$, or possibly studtite, $U^{VI}O_4 \cdot 4H_2O$ [22]. Interestingly, when H_2O_2 decomposition became partially blocked in this manner, there was a slight increase in the release of soluble $U^{VI}O_2^{2+}$ to the solution, Fig. 9.

For $[H_2O_2] \leq$ 0.01 mol L^{-1} and a sufficient $[CO_3]_{tot}$ to maintain access to the catalytic layer, H_2O_2 decomposition occurred under redox buffered conditions typified by an increase in rate (R_P^{-1}) with $[H_2O_2]$, while E_{CORR} remained constant, Fig. 6(A). Similar behavior was previously observed on undoped UO_2 [9] containing no noble metal (ϵ) particles, indicating that the role of the ϵ-particles in H_2O_2 decomposition was probably minor, although this remains to be demonstrated.

Under redox buffered conditions, the equilibrium potentials for the two half-reactions exhibit dependences on $[H_2O_2]$ which are similar but opposite in sign. Thus, provided both reactions were rapid, as would be the case on the catalytic $U^{IV}_{1-2x}U^{V}_{2x}O_{2+x}$ layer,

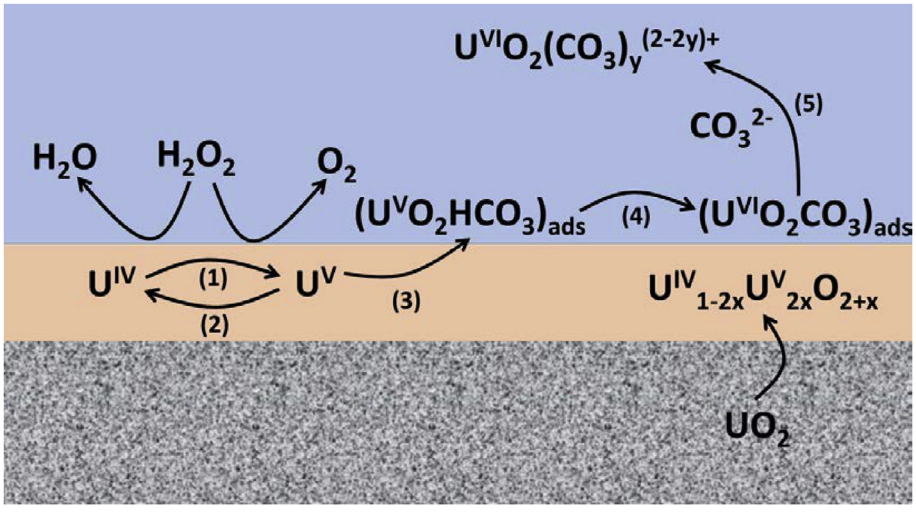

Fig. 10. A schematic illustration of the reactions involving H_2O_2 on a UO_2 surface.

the rate, but not E_{CORR}, would change with $[H_2O_2]$, as observed.

However, for $[H_2O_2] \geq 0.01$ mol L^{-1} the interfacial rate (the H_2O_2 consumption rate, but not necessarily the decomposition rate) became constant, while E_{CORR} increased. This would be expected to influence the relative kinetic importance of UO_2 corrosion and H_2O_2 decomposition by accelerating the sequence of reactions (3–5 in Fig. 10) leading to anodic dissolution of the UO_2 matrix, while retarding the transformation of U^V to U^{IV} (reaction 2, Fig. 10), the redox reaction catalyzing the decomposition cathodic half-reaction. This claim is consistent with our electrochemical results [24], which demonstrated that an increase in potential led to a much larger fraction of the anodic current (up to 40%) going to the anodic dissolution reaction.

5. Summary

- In aqueous HCO_3^-/CO_3^{2-} solutions in the presence of SIMFUEL, H_2O_2 consumption proceeded by homogenous decomposition in solution and by reaction with the SIMFUEL surface.
- Homogenous decomposition to O_2 and H_2O proceeded through a peroxycarbonate (CO_4^{2-}) intermediate, with a rate dependent on both $[CO_3]_{tot}$ and pH.
- On the SIMFUEL surface, H_2O_2 decomposition was the dominant reaction, with only minor to negligible amounts of UO_2 corrosion occurring. The stability of the SIMFUEL surface could be attributed to the stabilization of the $U^{IV}O_2$ matrix by RE^{III} doping.
- Surface decomposition proceeded via a radical mechanism and was catalyzed by the reversible $U^{IV} \rightleftharpoons U^V$ redox transition on a $U^{IV}_{1-2x}U^V_{2x}O_{2+x}$ surface.
- The primary function of HCO_3^-/CO_3^{2-} was to complex and dissolve U^{VI} surface species, which prevented their accumulation to form an insulating layer that blocked decomposition on the catalytic surface layer.
- When the surface was maintained free of U^{VI} species, H_2O_2 decomposition proceeded under redox buffered conditions on the catalytic surface.
- At high $[CO_3]_{tot}$ ($\geq$0.1 mol L^{-1}) and/or high $[H_2O_2]$ ($\geq$0.1 mol L^{-1}), the decomposition rate decreased, due to the more rapid formation of U^{VI} surface species that could be transferred to solution as $U^{VI}O_2(CO_3)_y^{(2-2y)+}$ by a chemical dissolution reaction.
- The role of noble metal (ϵ) particles in the SIMFUEL on H_2O_2 decomposition appears to be minor, although this remains to be conclusively demonstrated.

Declaration of competing interest

The authors declare that they have no known competing financial interests or personal relationships that could have appeared to influence the work reported in this paper.

CRediT authorship contribution statement

Ziyan Zhu: Methodology, Validation, Formal analysis, Investigation, Data curation, Writing - original draft, Visualization. **James J. Noël:** Methodology, Resources, Writing - review & editing, Supervision, Project administration, Funding acquisition. **David W. Shoesmith:** Conceptualization, Methodology, Resources, Writing - review & editing, Supervision, Project administration, Funding acquisition.

Acknowledgement

This research was funded under the Industrial Research Chair and Collaborative Research and Development grant (CRDPJ 507465–16) agreements between the Natural Sciences and Engineering Research Council of Canada (NSERC, Ottawa) and the Nuclear Waste Management Organization (NWMO, Toronto).

References

[1] P.G. Keech, P. Vo, S. Ramamurthy, J. Chen, R. Jacklin, D.W. Shoesmith, Design and development of copper coatings for long term storage of used nuclear fuel, Corrosion Eng. Sci. Technol. 49 (6) (2014) 425–430.
[2] D.S. Hall, P.G. Keech, An overview of the Canadian corrosion program for the long-term management of nuclear waste, Corrosion Eng. Sci. Technol. 52 (sup1) (2017) 2–5.
[3] T. Standish, J. Chen, R. Jacklin, P. Jakupi, S. Ramamurthy, D. Zagidulin, P. Keech, D. Shoesmith, Corrosion of copper-coated steel high level nuclear waste containers under permanent disposal conditions *Electrochim*, Acta 211 (2016) 331–342.
[4] G. Kwong, Status of Corrosion Studies for Copper Used Fuel Containers under Low Salinity Conditions. Report NWMO TR-2011-14, Nuclear Waste Management Organization, Toronto, ON, 2011.
[5] D. Shoesmith, Used Fuel and Uranium Dioxide Dissolution Studies–A Review. Report NWMO TR-2007-03, Nuclear Waste Management Organization, Toronto, ON, 2007.
[6] N. Liu, Z. Zhu, J.J. Noël, D.W. Shoesmith, Corrosion of nuclear fuel inside a failed waste container, Encyclopedia of Interfaical Chemistry: Surface Science and Electrochemistry 6 (2018) 172–182.
[7] E. Ekeroth, O. Roth, M. Jonsson, The relative impact of radiolysis products in radiation induced oxidative dissolution of UO_2, J. Nucl. Mater. 355 (1–3) (2006) 38–46.
[8] C.M. Lousada, M. Trummer, M. Jonsson, Reactivity of H_2O_2 towards different UO_2-based materials: the relative impact of radiolysis products revisited, J. Nucl. Mater. 434 (1–3) (2013) 434–439.
[9] S. Sunder, N.H. Miller, D.W. Shoesmith, Corrosion of uranium dioxide in hydrogen peroxide solutions, Corrosion Sci. 46 (5) (2004) 1095–1111.
[10] T.E. Eriksen, D.W. Shoesmith, M. Jonsson, Radiation induced dissolution of UO_2 based nuclear fuel – a critical review of predictive modelling approaches, J. Nucl. Mater. 420 (1–3) (2012) 409–423.
[11] C.M. Lousada, A.J. Johansson, T. Brinck, M. Jonsson, Mechanism of H_2O_2 decomposition on transition metal oxide surfaces, J. Phys. Chem. C 116 (17) (2012) 9533–9543.
[12] A. Barreiro Fidalgo, B. Dahlgren, T. Brinck, M. Jonsson, Surface reactions of H_2O_2, H_2, and O_2 in aqueous systems containing ZrO_2, J. Phys. Chem. C 120 (3) (2016) 1609–1614.
[13] C.M. Lousada, M. Yang, K. Nilsson, M. Jonsson, Catalytic decomposition of hydrogen peroxide on transition metal and lanthanide oxides, J. Mol. Catal. Chem. 379 (2013) 178–184.
[14] D. Fu, X. Zhang, P.G. Keech, D.W. Shoesmith, J.C. Wren, An electrochemical study of H_2O_2 decomposition on single-phase γ-FeOOH films, Electrochim. Acta 55 (11) (2010) 3787–3796.
[15] S.-S. Lin, M.D. Gurol, Catalytic decomposition of hydrogen peroxide on iron Oxide: kinetics, mechanism, and implications, Environ. Sci. Technol. 32 (10) (1998) 1417–1423.
[16] S. Nilsson, M. Jonsson, H_2O_2 and radiation induced dissolution of UO_2 and SIMFUEL pellets, J. Nucl. Mater. 410 (1–3) (2011) 89–93.
[17] P.G. Lucuta, R.A. Verrall, H. Matzke, B.J. Palmer, Microstructural features of SIMFUEL — simulated high-burnup UO_2-based nuclear fuel, J. Nucl. Mater. 178 (1) (1991) 48–60.
[18] M. Razdan, M. Trummer, D. Zagidulin, M. Jonsson, D.W. Shoesmith, Electrochemical and surface characterization of uranium dioxide containing rare-earth oxide (Y_2O_3) and metal (Pd) particles, Electrochim. Acta 130 (2014) 29–39.
[19] M. Razdan, D.W. Shoesmith, Influence of trivalent-dopants on the structural and electrochemical properties of uranium dioxide (UO_2), J. Electrochem. Soc. 161 (3) (2014) H105–H113.
[20] N. Liu, H. He, J.J. Noël, D.W. Shoesmith, The electrochemical study of Dy_2O_3 doped UO_2 in slightly alkaline sodium carbonate/bicarbonate and phosphate solutions, Electrochim. Acta 235 (2017) 654–663.
[21] N. Liu, J. Kim, J. Lee, Y.-S. Youn, J.-G. Kim, J.-Y. Kim, J.J. Noël, D.W. Shoesmith, Influence of Gd doping on the structure and electrochemical behavior of UO2, Electrochim. Acta 247 (2017) 496–504.
[22] L. Wu, D.W. Shoesmith, An electrochemical study of H_2O_2 oxidation and decomposition on simulated nuclear fuel (SIMFUEL), Electrochim. Acta 137 (2014) 83–90.
[23] M. Broczkowski, The effects of hydrogen and temperature on the electrochemistry and corrosion of uranium dioxide (UO_2), Ph.D. Thesis, The University of Western Ontario, 2008 (Chapter 7).
[24] Z. Zhu, L. Wu, J.J. Noël, D.W. Shoesmith, Anodic reactions occurring on simulated spent nuclear fuel (SIMFUEL) in hydrogen peroxide solutions containing bicarbonate/carbonate e the effect of fission products, Electrochim.

Acta 320 (10) (2019) 134546.
[25] R. Drot, E. Simoni, M. Alnot, J.J. Ehrhardt, Structural environment of uranium (VI) and europium (III) species sorbed onto phosphate surfaces: XPS and optical spectroscopy studies, J. Colloid Interface Sci. 205 (2) (1998) 410–416.
[26] A. Froideval, M. Del Nero, R. Barillon, J. Hommet, G. Mignot, pH dependence of uranyl retention in a quartz/solution system: an XPS study, J. Colloid Interface Sci. 266 (2) (2003) 221–235.
[27] T.B. Scott, G.C. Allen, P.J. Heard, M.G. Randell, Reduction of U(VI) to U(IV) on the surface of magnetite, Geochim. Cosmochim. Acta. 69 (24) (2005) 5639–5646.
[28] E.S. Ilton, J.-F. Boily, P.S. Bagus, Beam induced reduction of U(VI) during X-ray photoelectron spectroscopy: the utility of the U4f satellite structure for identifying uranium oxidation states in mixed valence uranium oxides, Surf. Sci. 601 (4) (2007) 908–916.
[29] B.G. Santos, H.W. Nesbitt, J.J. Noël, D.W. Shoesmith, X-ray photoelectron spectroscopy study of anodically oxidized SIMFUEL surfaces, Electrochim. Acta 49 (11) (2004) 1863–1873.
[30] M. Schindler, F.C. Hawthorne, M.S. Freund, P.C. Burns, XPS spectra of uranyl minerals and synthetic uranyl compounds. I: the U 4f spectrum, Geochem. Cosmochim. Acta 73 (9) (2009) 2471–2487.
[31] M. Razdan, D.S. Hall, P.G. Keech, D.W. Shoesmith, Electrochemical reduction of hydrogen peroxide on SIMFUEL (UO_2) in acidic pH conditions, Electrochim. Acta 83 (2012) 410–419.
[32] I. Štefanić, J.A. LaVerne, Temperature dependence of the hydrogen peroxide production in the γ-radiolysis of water, J. Phys. Chem. A 106 (2) (2002) 447–452.
[33] C.J. Hochanadel, Effects of Cobalt Y-Radiation on Water and Aqueous Solution, 1952.
[34] J. Abbot, D.G. Brown, Kinetics of Iron-catalyzed decomposition of hydrogen peroxide in alkaline solution, Int. J. Chem. Kinet. 22 (9) (1990) 963–974.
[35] W.D. Nicoll, A.F. Smith, Stability of dilute alkaline solutions of hydrogen peroxide, J. Ind. Eng. Chem. 47 (12) (1955) 2548–2554.
[36] O. Spalek, J. Balej, I. Paseka, Kinetics of the decomposition of hydrogen peroxide in alkaline solutions, J. Chem. Soc., Faraday Trans. 1: Physical Chemistry in Condensed Phases 78 (8) (1982) 2349–2359.
[37] R. Venkatachalapathy, G.P. Davila, J. Prakash, Catalytic decomposition of hydrogen peroxide in alkaline solutions, Electrochem. Commun. 1 (12) (1999) 614–617.
[38] E.L. Littauer, K.C.T, Catalytic decomposition of hydrogen peroxide in alkaline solution, J. Electrochem. Soc. 126 (11) (1979) 1924–1927.
[39] J. Flanagan, D.P. Jones, W.P. Griffith, A.C. Skapski, A.P. West, On the existence of peroxocarbonates in aqueous-solution, J. Chem. Soc., Chem. Commun. 1 (1986) 20–21.
[40] J.A. Navarro, M.A. de la Rosa, M. Roncel, F.F. de la Rosa, Carbon dioxide-mediated decomposition of hydrogen peroxide in alkaline solutions, J. Chem. Soc., Faraday Trans. 1: Physical Chemistry in Condensed Phases 80 (1) (1984) 249–253.
[41] D.W. Shoesmith, Fuel corrosion processes under waste disposal conditions, J. Nucl. Mater. 282 (1) (2000) 1–31.
[42] M. Razdan, D.W. Shoesmith, The electrocheical reacivity of 6.0 wt.% Gd doped UO_2 in aquous carbonate-bicarbonate solutions, J. Electrochem. Soc. 4 (161) (2014) H225–H234.
[43] B.G. Santos, J.J. Noël, D.W. Shoesmith, The effect of pH on the anodic dissolution of SIMFUEL (UO_2), J. Electroanal. Chem. 586 (1) (2006) 1–11.
[44] P.G. Keech, J.S. Goldik, Z. Qin, D.W. Shoesmith, The anodic dissolution of SIMFUEL (UO_2) in slightly alkaline sodium carbonate/bicarbonate solutions, Electrochim. Acta 56 (23) (2011) 7923–7930.